Programmable shape-morphing microrobots for localized cancer cells treatment

Chen Xin
University of Science and Technology of China
Dongdong Jin
The Chinese University of Hong Kong
Yanlei Hu
University of Science and Technology of China
Liang Yang
Institute of Nanotechnology Karlsruhe Institute of Technology
Rui Li
University of Science and Technology of China
Li Wang
University of Science and Technology of China
Zhongguo Ren
University of Science and Technology of China
Dawei Wang
University of Science and Technology of China
Shengyun Ji
University of Science and Technology of China
Kai Hu
University of Science and Technology of China
Deng Pan
University of Science and Technology of China
Hao Wu
CAS Key Laboratory of Mechanical Behavior and Design of Materials, Key Laboratory of Precision Scientific Instrumentation of Anhui Higher Education Institutes, Department of Precision Machinery and
Wulin Zhu
University of Science and Technology of China
Zuojun Shen
University of Science and Technology of China
Yucai Wang
University of Science and Technology of China
Jiawen Li
University of Science and Technology of China

Li Zhang
The Chinese University of Hong Kong https://orcid.org/0000-0003-1152-8962
Dong Wu (dongwu@ustc.edu.cn)
University of Science and Technology of China
Jiaru Chu
University of Science and Technology of China

Article

Keywords: shape morphing, microrobot, magnetic actuation, DOX release, Hela cells treatment

Posted Date: February 16th, 2021

DOI: https://doi.org/10.21203/rs.3.rs-198740/v1

Abstract

Microrobots have attracted great attentions due to their wide applications in microobjects manipulation and targeted drug delivery. To realize more complex micro/nano cargos manipulation (e.g., encapsulation and release) in biological applications, endowing microrobots with shapes adaptability with the environment is highly desirable. Here, designable shape-morphing microrobots (SMMRs) have been developed by programmatically encoding different expansion rate in a pH-responsive hydrogel. Combined with magnetic propelling, the shape-morphing microcrab (SMMC) is capable of performing targeted microparticle delivery, including gripping, transporting, and releasing through claws morphing. As a proof-of-concept demonstration, the shape-morphing microfish (SMMF) is designed to encapsulate drug (doxorubicin (DOX)) by closing mouth in phosphate buffer saline (PBS, pH~7.4) and release them by opening mouth in slightly acid solution (pH<7), which realize localized Hela cells treatment in an artificial vascular network. These SMMRs with powerful shape morphing capabilities and remote motion controllability provide new platforms for complex microcargos operation and on-demand drug release.

Introduction

Recently micro-nanorobots have become a hot topic due to their growing potential applications in targeted delivery[1-9], noninvasive surgery[10-13], biosensing[14-17], and detoxification[18-21]. With the development of micro and nano manufacturing technology, diverse robots from nanometer to micrometer scale have been fabricated [22-24]. To give the microrobots dynamical moving ability, a variety of propelling methods, such as chemical[16,19-20], ultrasonic[14-5,21], biological[25, 26], and magnetic driving mode[1-6] have been proposed. Among them, magnetic-driven approach receives widespread attention due to its precise guidance, wireless control, and strong ability to penetrate the human body. Thus, various magnetic microswimmers have been developed for various applications[27-33]. For example, using silica dioxide microspheres as templates, magnetic microrollers were fabricated by a multi-step metal deposition method, which were effectively propelled in a dynamic blood environment[27]. In addition, magnetic peanut-shaped motors were synthesized by hydrothermal process for manipulating and patterning of cells[28]. Moreover, several magnetic microhelix robots based on various materials (SU8, PEGDA, and GelMA) were printed by femtosecond laser direct writing (Fs-DLW) to achieve microparticles manipulation and targeted drug delivery[29-32]. Though ceaseless efforts have been dedicated to advancing the investigation of magnetic propelling microrobots, further development of functional microrobots based on stimuli responsive materials are highly desirable. They can response to the dynamic environment for more complex operation, such as microcargos clamping and unclamping, nanocargos encapsulating and releasing in biomedical fields.

Compared with traditional 3D printing, 4D printing based on stimuli responsive materials (e.g., liquid crystal polymers[34-38], responsive hydrogels[39-45], and other responsive biomaterials[46, 47]) introduces additional dimension to change the shape of 3D printed object for high functionality. Among these smart materials, hydrogel shows the advantages of high biocompatibility, tunable toughness, strong loading

capacity and low cost, and thus it is widely used for fabricating shape-morphing structures at microscale[48-51]. For example, several studies have been reported on fabricating shape-morphing structures based on stimuli-responsive hydrogels by Fs-DLW, which still remain two main limitations, 1) Present structures including micro stent, umbrella, and cantilever are static, which only perform simple operations without remote manipulating property. 2) 4D printed structures have been used to realize various applications, such as smart compound eyes for tunable imaging, flexible microgripper for particles capture in the same position. However, further specific biomedical applications (e.g., targeted drug therapy, stem cell transportation) have not yet appeared.

Herein, programmable magnetic microrobots with changeable shapes are developed by one-step 4D laser printing in one kind of pH-responsive hydrogel, which can realize complex functions including complicated microparticle operation (gripping, transporting, and releasing), the drug (DOX) encapsulating and controllable releasing in specific location for cancer cells treatment. Based on adjusting processing parameters, programmatically encoding shape morphing is realized by controlling the expansion rate in localized part of SMMRs, which is determined by the part porosity. Therefore, several kinds of SMMRs with controllable morphing extent and fast response speed (<300 ms) are fabricated including SMMF, SMMC, and shape-morphing microbutterfly (SMMB). Subsequently, the printed SMMRs are endowed with magnetic control capabilities through magnetite nanoparticles (Fe_3O_4 NPs) solution immersion. Most importantly, the responsive pH value of SMMF decreases from the original value of 9 in NaOH to the value of 7.4 in the PBS, which is crucial for biomedical applications. Thus, taking advantages of predictable shape morphing capability and remote magnetic control, diverse applications are achieved, such as microparticles operation and controllable DOX releasing to treat Hela cells. These SMMRs with magnetic propelling capabilities and switchable shapes will find broad potential prospects for applications in complicated single cell manipulation (picking/placing) and controllable drug releasing for on-demand cancer cells treatment.

One-step 4D printing of SMMRs for Hela cells treatment

Inspired by natural fish switching mouth shape (opening/closing), smart SMMF with shape-morphing mouth is designed for encapsulating and controllable releasing DOX into Hela cells **(Figure 1a**). In this work, all of the SMMRs are printed in one kind of pH-responsive hydrogel, which mainly contains functional acrylic acid (AAc), the cross-linker dipentaerythritol pentaacrylate (DPEPA), and photoinitiator 4,4’-bis (diethylamino) benzophenone (EMK) (Figure 1b). At high pH value environment (pH>9), these carboxyl groups become deprotonated and negatively charged, which will generate electrostatic repulsion forces between molecular chains, resulting in significant expansion of the hydrogel network. Inversely, when the carboxyl groups are protonated at low pH value (pH<9), the network collapses resulting in the hydrogel shrinkage.

The SMMRs are fabricated using an Fs-DLW system (Figure 1c, Figure S1), where programmable morphing is realized by adjusting the scanning point density in localized part of SMMRs. For example, the SMMF is printed along the most optimized scanning path (Figure S2), where the scanning point

density of the edge part of fishtail is 2.5 times that of the middle part. As expected, at low pH value, the tail of SMMF shows anisotropic shrinkage from edge to middle due to the different localized point densities (500 nm and 200 nm), while the body of SMMF has the same denser scanning point (200 nm) leading to slight isotropic contraction. In order to explain the morphing mechanism of hydrogel, gel pores in different point density parts are measured. As shown in Figure 1d, the average pore area (5393 nm^2) in the denser scanning point part is much smaller than that (14591 nm^2) in the looser scanning point part according to image processing results (Figure S3). The results indicate that the region with a larger point spacing is subject to bigger stress during dehydration resulting in larger morphing. Based on shape morphing theoretical analysis, the SMMF and SMMC are fabricated by encoding the scanning point density. As illustrated in Figure 1e, the SMMF's fins and SMMC's claws consist of two parts, where the light red part represents loose point part and the deep red part represents dense point part. As designed, the SMMF and SMMC can quickly open and close their fins and claws by switching pH value (Figure S4, Video 1), respectively. According to the optical images, both of SMMF fins and SMMC claws complete designed morphing by pH switching and the SMMF morphing shows fast response speed (~300 ms) by each frame analysis (Figure S5). Meanwhile, the shape morphing also has strong repeatability, which can stably complete over 50 cycles (Figure S6). Compared with previous robots, these microscale (10~100 mm) SMMRs show several advantages including programmable shape conversion based on one kind of stimulus responsive material and one-step rapid fabrication process (laser scanning time < 5 mins).

Programmable shape morphing of microrobots

In order to gain a deeper understanding of the SMMRs shape morphing, it is of great significance to conduct quantitative research on the process parameters. Here, cantilever structure is chosen as a representative model to analyze the relationship between morphing extent and various parameters. In our work, the structures are point-to-point scanned by inputting the point coordinates of the X and Y directions into the scanning galvanometer, and different point densities can be achieved by adjusting the distance between two adjacent coordinates during processing. For the microcantilever fabrication, the point spacing in one part is bigger than that of another part (**Figure 2a)**, leading to different scanning point densities in each single slice and ultimately bending. Here, the bending angle (θ), defined as vertical (Y) to horizontal (X) distance ratio between the tip point and the root of the microcantilever, is used to characterize the extent of anisotropic shape morphing, which can be calculated as:

$$\theta = tan^{-1}\frac{Y}{X} \quad (1)$$

As shown in figure 2b, the microcantilever swells in high pH value solution and even shows a little reverse bending because of the internal stress, caused by different point densities. By contrast, under low pH value, the microcantilever bends to the designed direction owing to carboxylic groups in AAc releasing protons (Video 2). In particular, scanning point spacing ratio (SPSR), the volume of loose part to total

volume ratio (VR), and aspect ratio (AR) are quantitatively investigated, which are three most important factors for bending angle.

Firstly, cantilever structure is divided into two parts with different point spacing to regulate the SPSR, which is defined as:

$$\mathrm{SPSR} = \frac{PS_l}{PS_d} \quad (4)$$

Where PS_l and PS_d are point spacing in the loose and dense part, respectively. When point spacing in two parts are the same (SPSR=1), the microcantilever remains horizontal. The maximum bending angle can reach as much as 74° with the SPSR of 2.5 (Figure 2c). However, the bending angle reduces to nearly zero again when the SPSR increases over 3, because adjacent points cannot effectively connect together to provide enough shrinkage (Figure S8). In addition, the VR as an important parameter affecting the bending angle has also been studied in detail. Due to the same length and height of the cantilever, the VR could be calculated as:

$$\mathrm{VR} = \frac{W_l}{W} \quad (2)$$

Where W_l and W are the loose part and total width of the microcantilever, respectively. Experimental results show that when the VR reaches 0.8, the bending angle increases to 74° (Figure 2d). However, when VR continues to increase to 0.9, the microcantilever cannot fully have repeatable shape morphing due to low-strength structures (Figure S9). Besides, the AR of the microcantilever also has an important influence on the maximum bending angle, which is defined as:

$$\mathrm{AR} = \frac{L}{W} \quad (3)$$

Where W and L are the width and length of the microcantilever, respectively. As expected, the bending angles have positive correlation with the ARs, where the bending angle is up to 82° with AR of 14 (Figure 2e, Figure S10).

Combining structural design and process optimization, microstructures with controllable morphing direction and extent are realized (Figure S11). For example, the inward and outward bending microstructures are demonstrated (Figure 2f-h). Furthermore, the composite structures (stamen) at microscale with both inward and outward bending can also be fabricated (Figure 2i, Video 3-4). These investigations of controllable morphing provide a solid foundation for encoding complex microrobots. Inspired by natural animals, three dimensional (3D) SMMRs (SMMC and SMMB) with specific shape morphing capability are designed and fabricated (Figure 2j). Both of their claws and wings have two parts with 200 nm and 500 nm scanning point spacing so that they can accurately complete

programmable morphing similar to real natural animals with the change of pH value. For the morphing simulation analysis, finite element simulation model is carried out by introducing a volumetric stress. Specifically, two constituent materials A1 and A2 are distinguished by different scanning point spacing in such way that the numerical results closely resemble the experimental morphing. The measured volume expansion rates are αA1 = −0.48 and αA2 = −0.27 in looser and denser laser scanning area, respectively. Based on the coupling of solid mechanics and solid heat transfer, the shapes of the microrobots after morphing are simulated, and the morphing degree is consistent with the simulation result (Figure S12-13). The SMMC shows its claws morphing similar to real crab hunting for food, where the claw width increases from 3 μm up to 14 μm. Moreover, the SMMB also can swell in high pH value in order to flap wings from 50 μm to 91 μm (Figure 2k). These SMMRs demonstrate that natural typical creatures with distinct shape morphing characteristics could be mimicked.

Magnetic SMMC for gripping, transporting and releasing microparticle by claws morphing

As a fuel-free, wireless, and non-pollution propelling method with high controllability, magnetic propelling can help SMMRs achieve more tasks in dynamic environment. Therefore, the SMMC with localized transformable claws is fabricated, and targeted microcargo manipulation is completed by magnetic control. Firstly, the SMMC is developed by one-step 4D printing and is immersed in Fe_3O_4 NPs suspension in order to introduce magnetic driving capability (**Figure 3a**). Here, Fe_3O_4 NPs are wrapped in silica shells to avoid reacting with hydrochloric acid (Figure S14). The NPs can be clearly observed on the surface of SMMC by elemental analysis, where iron (Fe) and silicon (Si) are shown in figure 3c-f, respectively. Subsequently, the samples are cleaned several times in ethanol for cargo manipulation.

As shown in figure 3g-h, the SMMC claws covered with nanoparticles still have great morphing properties (from 2 μm to 14 μm), which are enough to complete cargo griping. In order to integrate with commercial equipment (e.g., biological culture boxes and inverted fluorescence microscopes) for complex applications, two permanent ferromagnets are used for remote actuation, which applies a magnetic force on the magnetized SMMC. To demonstrate the precise propelling of magnetic SMMC, the trajectory patterns of “V” and “good” are followed by adjusting SMMC propelling direction (Figure 3b, Figure S15). Besides, the average propelling speed of SMMRs can reach 60 $\mu m \cdot s^{-1}$ (Figure S16). Taking advantages of designed shape morphing and precise propelling capabilities, SMMC is successfully actuated for targeted cargo gripping, transporting, and releasing, as shown in schematic illustration and time-lapse optical images (Figure 3i-j). At first, the SMMC slowly approaches to the targeted cargo (10 μm silica microsphere) and traps it in the center of the claws (the enlarged image in Figure 3j). Dilute hydrochloric acid is subsequently added to adjust the pH value lower than 9 so that the crab claws shrink to tightly grip the target microparticle, which avoids cargo loss during transportation. Finally, the SMMC completes the cargo delivery by external magnetic field, and opens its claws at target position for cargo releasing (Video 5) when sodium hydroxide is added to adjust the pH value higher than 9. Compared with conventional microrobots that cannot grasp and easily leak cargo, thus they can only complete 2D trajectory movement[52], this SMMC can actively grasp and manipulate microcargos in 3D space, and release it at target locations. This phenomenon is verified from video 5, where the SMMC can still tightly

capture the cargo even when it flips up and down. Thus, the SMMC holds great promise for manipulation of microcargos in biomedical research. However, due to the limitation of morphing critical pH~9, the responsive microrobots are unable to complete biomedical applications under physiological conditions (pH~7.4).

Magnetic SMMF encapsulating and controllable releasing drug (DOX) by mouth morphing

In this study, we are pleasantly surprised to discover that the synthetic hydrogel could also realize morphing in the PBS, where pH value is 7.4. The PBS solution is composed of NaCl, KCl, Na_2HPO_4, and KH_2PO_4. Therefore, the SMMF morphing in above four solutions is separately tested when their pH values are adjusted to ~7.4 by adding NaOH/HCl, and it is found that the SMMF swells in KH_2PO4 and Na_2HPO_4 (pH=7.4) (Figure S17). Based on these systematic tests, we suppose that HPO_4^{2-} and HPO_4^{-} partially break the original hydrogen bonds between PNIPAAm and PAAc, which lead to the deprotonation of carboxyl groups of the hydrogel in the PBS solution (Figure 4b). The responsive morphing pH value decreases from the original 9 in NaOH to 7.4 in the PBS, which is the key for subsequent biological applications (Figure 4c).

Precise control of the drug releasing is highly desirable for targeted therapy however remains challenging for microrobots[9,51]. For example, although magnetic microswimmers have been developed for targeted drug delivery to treat cancer cells, the release of drug molecules grafted on its surface occurs at any time because they are always exposed to the solution. Here, microfish with adjustable mouth morphing is designed for encapsulation and controllable drug release *in vitro* (**Figure 4a**). The drug we chose is one kind of homemade DOX-loaded nanoparticle (DOX NP ~120 nm) encapsulated by poly (2-azepane ethyl methacrylate)-block-poly (ethyl acrylate of lipoicacid), which can treat the Hela cells (Figure S18). By optimizing structural design, SMMF opens its mouth at pH<7, creating a 2 μm hole to facilitate drug loading (Figure 4d). The SMMF is immersed into the suspension of drug NPs (opening mouth) for 10 minutes to load them into hollow body. Subsequently, the SMMF closes its mouth to encapsulate drug NPs by adding the PBS solution. After washing several times, the drug NPs on the fish surface are washed out while those in the fish body are effectively encapsulated, which is verified by the red fluorescence. Similar to the aforementioned magnetic SMMC, superparamagnetic nanoparticles are adhered to SMMF by immersion treatment for remote magnetic control. The magnetic SMMF is transferred to the cell culture dish by a microliter pipette, which is performed in a biological safety cabinet to prevent cell contamination. Under the dynamic control of permanent ferromagnets, the magnetic SMMF is controllably steered in the Hela cell clusters. Since the SMMF does not adhere to the Hela cells during the movement, it can move along a rectangular trajectory within 30 s, which provides a basis for subsequent targeted drug delivery (Figure 4e, Video 6). In order to prove that SMMF can achieve controllable drug encapsulation and release through the mouth switch, we conduct three sets of controlled experiments (i, The SMMF with DOX and opening mouth, ii, The SMMF without DOX and opening mouth, and iii, The SMMF with DOX and closing mouth) (Figure 4f). Under the situation (i), the DOX rapidly releases from fish mouth and kills the Hela cells around it. It's observed that DOX diffuse

range has positive relationship with time. Over a period of 6 hours, the red fluorescence of DOX appears on the cell, which is 250 μm away from the SMMF (Figure 4g, Video 7). Meanwhile, during several hours of cultivating in the live cell workstation, the red fluorescence of DOX in Hela cells keeps increasing, while the green fluorescence from Hela cells gradually fades, indicating that the release of DOX has an effective damage on Hela cells. Quantitative analysis indicates about 80% enhancement of fluorescence intensity of DOX in cells after 6 hours (Figure 4h). As control groups, Hela cells normally grow and proliferate around SMMF (under the situation ii), showing that the hydrogel itself has no effect on cell viability (Figure S19). Furthermore, in order to verify the ability of fish mouth to encapsulate DOX, the SMMF (under the situation iii) is put in Hela cells over 6 hours. It can be seen that Hela cells do not show red DOX fluorescence, and the green fluorescence of Hela cells are basically unchanged. These experiments show that the SMMF can achieve switch of DOX encapsulation and release through closing and opening mouth in the liquid from pH<7.4 to 7. As previously work reported, the pH value in normal environment of the human body is 7.4, while the tumor region is <7[53, 54]. Therefore, the SMMF will provide a good prospect for controllable drug release in tumor area through shape conversion.

Localized Hela cells treatment in a complex network using magnetic SMMF

To demonstrate the feasibility of localized cancer cells treatment by magnetic SMMF, we manipulate SMMF loaded with DOX in an artificial vascular network to treat Hela cells in target area. Here, the complex network is prepared from mask UV lithography and Polydimethylsiloxane (PDMS) replica molding (**Figure 5a**). Each microchannel has a width of 70 ~ 150 μm and a depth of 80 μm which is suitable for swimming of an SMMF (~50 μm). The network is firstly modified by plasma for better bonding to the cover glass. The network is subsequently soaked in the Poly-L-Lysine (PLL) solution over 2 hours, which helps Hela cells better adhere to the channel. The nutrient medium containing Hela cells is blown several times and dropped on the network. After 2 days of culture, Hela cells almost covered the entire network for subsequent drug delivery. The magnetic SMMF swims along the network under the control of external magnetic field (Figure 5b, Video 8), stops at a target position in network, and opens mouth to release DOX by adding a mixture of hydrochloric acid and medium (pH<7). We define the area where microfish exists as the drug release area, while the other channels are control area. Over a period of 6 hours, the DOX in SMMF body quickly diffuses to the surrounding Hela cells, causing the green fluorescence in cells to gradually extinguish (Figure 5c). By contrast, the Hela cells in other control channels grow and proliferate normally, without any red DOX fluorescent molecules (Figure 5d). Furthermore, we quantitatively analyze the relationship between DOX red fluorescence intensity and time, where the normalized intensity of DOX in Hela cells grows from 7% to 78% (Figure 5e). Meanwhile, compared with drug release area, the green fluorescence intensity of Hera cells decreases to 10%, while that in the control area remains at 80% after 6 hours (Figure 5f). Such SMMF realizes the encapsulation and controllable release of DOX by mouth shape conversion, and promotes it for on-demand cancer cells treatment by combining with remote magnetic propelling property, which provides a brand-new platform for cancer research.

Conclusions

In this work, magnetic SMMRs showing wireless motion control and designable morphing are proposed, which realize microparticles operation and localized drug (DOX) encapsulating/releasing with high spatial and temporal resolution. Compared with conventional microrobots, these SMMRs have powerful deformability realized by encoding the scanning density in localized part in one kind of pH responsive hydrogel. Based on repeatable shape switch of SMMRs, the SMMC is used to achieve the picking and releasing operation of 10 μm silica particles by claws morphing. In addition, we found that the SMMF can respond to the PBS with pH~7.4, which enables the possibility of biomedical applications. Thus, the SMMF is used for loading and releasing of drug by mouth shape conversion for cancer cells treatment in target area, which is quantitatively studied by comparing the fluorescence changes of Hela cells and DOX in different areas in an artificial vascular networks. This work offers a flexible and one-step method for manufacturing microrobots with advantages of changeable shapes, magnetic remote controllability, and high biocompatibility, which provides a versatile platform for the drug encapsulation and releasing for further cancer therapy.

Methods

Preparation of pH-responsive hydrogel.

Firstly, 1.6 g N-isopropylacrylamide (NIPAAm, 98%), 0.8 mL Acrylic acid (AAc, 99%), and 0.15 g polyvinylpyrrolidone (PVP, average Mw ~1, 300, 000) are added to 1 mL ethyl lactate (EL, 98%) and then stirred vigorously. Then, 2.5 mL of the above solution, 0.5 mL dipentaerythritol hexaacrylate (DPEHA,98%), 0.5 mL triethanolamine (TEA, 99%), and 100 μL 4,4-bis(diethylamino) benzophenone (EMK, 97%) / N, N-dimethylformamide (DMF, 99.5%) solution (20 wt.%) are mixed, followed by stirring 12 h, to mix each component completely. Finally, the precursor is kept in yellow light condition to avoid unnecessary light exposure.

Design and fabrication of magnetic SMMRs

Typical femtosecond laser writing system source is a mode-locked Ti: sapphire laser oscillator (Chameleon Vision-S, Coherent Corp, central wavelength: 800 nm, repetition rate: 80 MHz, pulse width: 75 fs). Firstly, processing is performed using femtosecond laser direct writing technology. The polymer molecular chains at the laser focus are polymerized. The processed sample is immersed in a developing solution (ethanol or isopropyl alcohol) for 15 minutes to remove the uncured hydrogel. The developed sample is then taken out and placed under an inverted microscope for in-situ observation. In order to avoid the fast evaporation of ethanol, pure water is dripped around the sample. When the NaOH solution is dropped, the sample swells, and then dilute hydrochloric acid is added dropwise to make the sample shrink.

Remote magnetic control of SMMRs

After one-step 4D printing of SMMRs, the sample is immersed in the magnetic particles (NPs) suspension cultured 12 h in order to absorb nanoparticles. Subsequently, we use a home-made three-dimensional mobile platform and capillary microneedle to peel off the micro-robot and transfer it with a microliter pipette. At last, the magnetic actuation of SMMRs is realized by two permanent magnets.

Characterization

Optical micrographs are taken with an inverted fluorescence microscope (Leica DMI3000b). The SEM images are collected with a secondary electron SEM (ZEISS EVO18) operated at an accelerating voltage of 10 keV after depositing ~10 nm gold. The Energy Dispersive Spectrometer (EDS) analysis spectroscopy images are obtained on COLD FESEM (Hitachi, SU8220).

Cell Culture

Hela-EGFP cells are obtained from American Type Culture Collection and cultured in a humidified atmosphere at 37 °C with 5% CO2. The cells are cultured in normal Dulbecco's modified eagle medium (Gibco, Thermo Fisher Scientific, Grand Island, NY) supplemented with 10% fetal bovine serum (HyClone, Logan, UT) and 1% penicillin/streptomycin (Gibco, Life Technologies, Grand Island, NY). For cells therapeutic experiment, Hela cells are detached from culture dish by trypsinization with 0.25% Trypsin-EDTA (Gibco, USA) at 37 °C for 30 s, centrifuged at 1000 rpm for 5 min. Then cells are resuspended in culture medium at a density of 2 × 10 6 mL^{-1} for use.

Preparation of drug (DOX-loaded NPs)

Poly (ethylene glycol)-block-poly (2-azepane ethyl methacrylate) (PEG-*b*-PAEMA) diblock copolymer is synthesized by RAFT polymerization of AEMA using PEG-based macro chain transfer agent, poly (ethylene glycol) conjugated 4-cyanopentanoic acid dithiobenzoate (PEG-CPAD). Briefly, PEG-CPAD (0.26 g, 1.0 eqv), monomer AEMA (1.57 g, 141 eqv), and AIBN (2.4 mg, 0.32 eqv) are dissolved in dioxane. After freezing and thawing for 3 times, the mixture is stirred at 75 °C for 8 h. The resulting copolymer is isolated by precipitation in cold hexane and dried under vacuum (61% yield). To prepare DOX encapsulated polymeric nanomedicine by PEG-b-PAEMA, 1 mg hydrophobic DOX is dissolved in DMSO and 20 mg PEG-b-PAEMA is added. After stirring for 5 min, 10 mL ultrapure water is added and the solution kept stirring for 10 min. The DOX encapsulated nanoparticles are dialyzed against water and stored at 4 °C.

Declarations

Acknowledgment

This work was supported by the National Natural Science Foundation of China (Nos. 61927814, 91963127, 51675503, 51875544, 51805508, 51805509, 52075516, 62005262, 52005475), National Key R&D Program of China (2017YFB1104303, 2018YFB1105400), Major Scientific and Technological

Projects in Anhui Province (201903a05020005), the Fundamental Research Funds for the Central Universities (YD2090002005, WK2090050048, WK 2090000001), and Youth Innovation Promotion Association CAS (2017495)

We acknowledge the Experimental Center of Engineering and Material Sciences at USTC for the fabrication and measuring of samples. This work was partly carried out at the USTC Center for Micro and Nanoscale Research and Fabrication.

L.Z. thanks the financial support from the Hong Kong Research Grants Council (RGC) with project No. JLFS/E-402/18, CAS-Croucher Funding Scheme for Joint Laboratories with project No. CAS20403, the ITF project with Project No. MRP/036/18X funded by the HKSAR Innovation and Technology Commission (ITC), and the support from Multi-scale Medical Robotics Center (MRC), InnoHK, at the Hong Kong Science Park.

Author contributions

C.X., D.W., and L.Z. conceived the idea and designed the project. C.X., D.-D. J., D.-W. W., Z.-G. R., and L.W. performed all the experiments and the characterization. C.X., Y.-L.H., L.Y., D.P., and W.-L. Z. completed data analysis and figure depicture. R.L., and S.-Y.J. helped for setting up 4D printing system. K.H. and H.W. provided assistance on the artificial network fabrication. Z.-J.S., and Y.-C.W., designed biomedical experiment. C.X., D.W., and J.-W.L. wrote and revised the paper. D.W., L.Z., and J.-R.C. supervised the project.

Additional information

Supplementary Information is available in the online version of the paper

References

1. Li, J., et al. Development of a magnetic microrobot for carrying and delivering targeted cells. *Sci. Robot.* **3**, (2018)
2. Jeon, S., et al. Magnetically actuated microrobots as a platform for stem cell transplantation. *Sci. Robot.* **4**, (2019)
3. Tottori, S., et al. Magnetic helical micromachines: fabrication, controlled swimming, and cargo transport. *Adv. Mater.* **24**, 811-6 (2012)
4. Servant, A., et al. Controlled in vivo swimming of a swarm of bacteria-like microrobotic flagella. *Adv. Mater.* **27**, 2981-8 (2015)
5. Felfoul, O., et al. Magneto-aerotactic bacteria deliver drug-containing nanoliposomes to tumour hypoxic regions. *Nat. Nanotechnol.* **11**, 941-947 (2016)
6. Li, J., et al. Enteric Micromotor Can Selectively Position and Spontaneously Propel in the Gastrointestinal Tract. *ACS Nano*. **10**, 9536-9542 (2016)

7. Wang, B., Kostarelos, K., Nelson, B. J.,Zhang, L. Trends in Micro-/Nanorobotics: Materials Development, Actuation, Localization, and System Integration for Biomedical Applications. *Adv. Mater.* 2002047 (2020)
8. Li, J., et al. Micro/nanorobots for biomedicine: Delivery, surgery, sensing, and detoxification. **2**, (2017)
9. Wang, Q.,Zhang, L. External Power-Driven Microrobotic Swarm: From Fundamental Understanding to Imaging-Guided Delivery. *ACS Nano*. (2021)
10. Srivastava, S. K., Medina-Sanchez, M., Koch, B.,Schmidt, O. G. Medibots: Dual-Action Biogenic Microdaggers for Single-Cell Surgery and Drug Release. *Adv. Mater.* **28**, 832-7 (2016)
11. Leong, T. G., et al. Tetherless thermobiochemically actuated microgrippers. *Proc. Natl. Acad. Sci. USA*. **106**, 703-708 (2009)
12. Kagan, D., et al. Acoustic droplet vaporization and propulsion of perfluorocarbon-loaded microbullets for targeted tissue penetration and deformation. *Angew. Chem. Int. Ed. Engl.* **51**, 7519-22 (2012)
13. Chatzipirpiridis, G., et al. Electroforming of implantable tubular magnetic microrobots for wireless ophthalmologic applications. *Adv. Healthc. Mater.* **4**, 209-14 (2015)
14. Esteban-Fernández de Ávila, B., et al. Single cell real-time miRNAs sensing based on nanomotors. *ACS Nano*. **9**, 6756-6764 (2015)
15. Morales-Narvaez, E., et al. Micromotor enhanced microarray technology for protein detection. *Small*. **10**, 2542-8 (2014)
16. Pacheco, M., Jurado-Sanchez, B.,Escarpa, A. Sensitive Monitoring of Enterobacterial Contamination of Food Using Self-Propelled Janus Microsensors. *Anal. Chem.* **90**, 2912-2917 (2018)
17. Zhang, Y., et al. Real-time tracking of fluorescent magnetic spore–based microrobots for remote detection of C. diff toxins. *Sci. Adv.* **5**, eaau9650 (2019)
18. Hu, C. M., et al. A biomimetic nanosponge that absorbs pore-forming toxins. *Nat. Nanotechnol.* **8**, 336-40 (2013)
19. Zhu, W., et al. 3D-Printed Artificial Microfish. *Adv. Mater.* **27**, 4411-4417 (2015)
20. Vilela, D., et al. Graphene-Based Microbots for Toxic Heavy Metal Removal and Recovery from Water. *Nano. Lett.* **16**, 2860-6 (2016)
21. de Ávila, B. E.-F., et al. Hybrid biomembrane–functionalized nanorobots for concurrent removal of pathogenic bacteria and toxins. *Sci. Robot.* **3**, eaat0485 (2018)
22. Li, J.,Pumera, M. 3D printing of functional microrobots. *Chem. Soc. Rev.* (2021)
23. Palagi, S.,Fischer, P. Bioinspired microrobots. *Nat. Rev. Mater.* **3**, 113-124 (2018)
24. Jin, D.,Zhang, L. Embodied intelligence weaves a better future. *Nat. Mach. Intell.* **2**, 663-664 (2020)
25. Magdanz, V., Sanchez, S.,Schmidt, O. G. Development of a sperm-flagella driven micro-bio-robot. *Adv. Mater.* **25**, 6581-6588 (2013)
26. Medina-Sánchez, M., et al. Cellular cargo delivery: Toward assisted fertilization by sperm-carrying micromotors. *Nano. Lett.* **16**, 555-561 (2016)

27. Alapan, Y., et al. Multifunctional surface microrollers for targeted cargo delivery in physiological blood flow. *Sci. Robot.* **5**, (2020)
28. Lin, Z., et al. Magnetically actuated peanut colloid motors for cell manipulation and patterning. *ACS Nano*. **12**, 2539-2545 (2018)
29. Yasa, I. C., et al. 3D-Printed Microrobotic Transporters with Recapitulated Stem Cell Niche for Programmable and Active Cell Delivery. *Adv. Funct. Mater.* **29**, (2019)
30. Wang, X., et al. 3D Printed Enzymatically Biodegradable Soft Helical Microswimmers. *Adv. Funct. Mater.* **28**, (2018)
31. Ceylan, H., et al. 3D-Printed Biodegradable Microswimmer for Theranostic Cargo Delivery and Release. *ACS Nano*. **13**, 3353-3362 (2019)
32. Bozuyuk, U., et al. Light-Triggered Drug Release from 3D-Printed Magnetic Chitosan Microswimmers. *ACS Nano*. **12**, 9617-9625 (2018)
33. Yan, X., et al. Multifunctional biohybrid magnetite microrobots for imaging-guided therapy. *Sci. Robot.* **2**, (2017)
34. Kotikian, A., et al. Untethered soft robotic matter with passive control of shape morphing and propulsion. *Sci. Robot.* **4**, 7044 (2019)
35. Jin, B., et al. Programming a crystalline shape memory polymer network with thermo-and photo-reversible bonds toward a single-component soft robot. *Sci. Adv.* **4**, eaao3865 (2018)
36. Palagi, S., et al. Structured light enables biomimetic swimming and versatile locomotion of photoresponsive soft microrobots. *Nat. Mater.* **15**, 647-53 (2016)
37. Wani, O. M., Zeng, H.,Priimagi, A. A light-driven artificial flytrap. *Nat. Commun.* **8**, 15546 (2017)
38. Shahsavan, H., et al. Bioinspired underwater locomotion of light-driven liquid crystal gels. *Proc. Natl. Acad. Sci. USA*. **117**, 5125-5133 (2020)
39. Wang, Z., Li, K., He, Q.,Cai, S. A Light-Powered Ultralight Tensegrity Robot with High Deformability and Load Capacity. *Adv. Mater.* **31**, e1806849 (2019)
40. Zhang, H., Mourran, A.,Moller, M. Dynamic Switching of Helical Microgel Ribbons. *Nano. Lett.* **17**, 2010-2014 (2017)
41. Zhang, X., et al. Optically- and thermally-responsive programmable materials based on carbon nanotube-hydrogel polymer composites. *Nano. Lett.* **11**, 3239-44 (2011)
42. Zuo, B., Wang, M., Lin, B. P.,Yang, H. Visible and infrared three-wavelength modulated multi-directional actuators. *Nat. Commun.* **10**, 4539 (2019)
43. Zhao, Y., et al. Soft phototactic swimmer based on self-sustained hydrogel oscillator. *Sci. Robot.* **4**, (2019)
44. Kaehr, B.,Shear, J. B. Multiphoton fabrication of chemically responsive protein hydrogels for microactuation. *Proc. Natl. Acad. Sci. USA*. **105**, 8850-8854 (2008)
45. Li, H., et al. Magnetic actuated pH-responsive hydrogel-based soft micro-robot for targeted drug delivery. *Smart Mater. Struct.* **25**, (2016)

46. Morimoto, Y., Onoe, H.,Takeuchi, S. Biohybrid robot powered by an antagonistic pair of skeletal muscle tissues. *Sci. Robot.* **3**, (2018)
47. Sun, Y.-L., et al. Protein-based soft micro-optics fabricated by femtosecond laser direct writing. *Light: Sci. Appl.* **3**, e129 (2014)
48. Jin, D., et al. Four-dimensional direct laser writing of reconfigurable compound micromachines. *Mater. Today*. **32**, 19-25 (2020)
49. Hippler, M., et al. Controlling the shape of 3D microstructures by temperature and light. *Nat. Commun.* **10**, 232 (2019)
50. Zarzar, L. D., et al. Direct writing and actuation of three-dimensionally patterned hydrogel pads on micropillar supports. *Angew. Chem. Int. Ed. Engl.* **50**, 9356-60 (2011)
51. Tudor, A., et al. Fabrication of soft, stimulus-responsive structures with sub-micron resolution via two-photon polymerization of poly(ionic liquid)s. *Mater. Today*. **21**, 807-816 (2018)
52. Sattayasamitsathit, S., et al. Fully loaded micromotors for combinatorial delivery and autonomous release of cargoes. *ACS Nano*. **10**, 2830-2833 (2014)
53. Wang, Y., et al. A nanoparticle-based strategy for the imaging of a broad range of tumours by nonlinear amplification of microenvironment signals. *Nat. Mater.* **13**, 204-212 (2014)
54. Webb, B. A., Chimenti, M., Jacobson, M. P.,Barber, D. L. Dysregulated pH: a perfect storm for cancer progression. *Nat. Rev. Cancer*. **11**, 671-677 (2011)

Figures

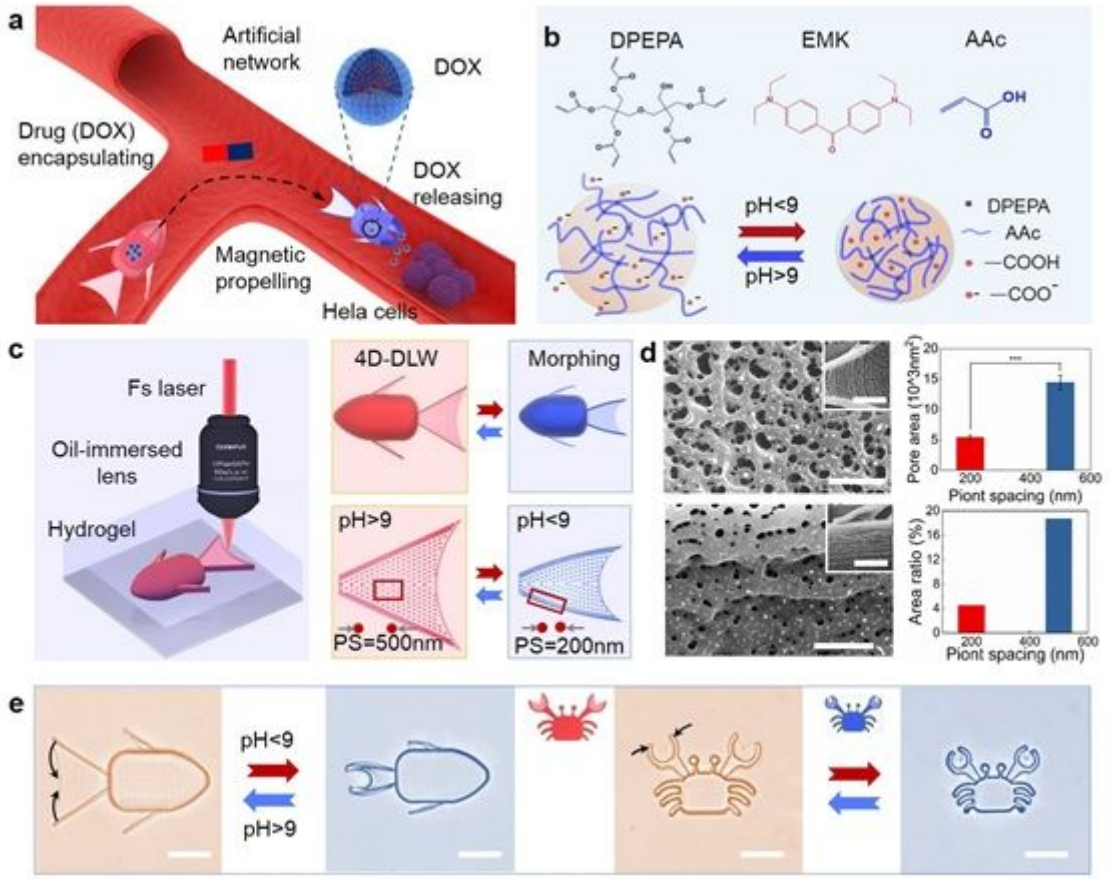

Figure 1

One-step 4D printing of SMMRs for Hela cells treatment. a Schematic illustration of magnetic SMMF for targeted DOX releasing to treat cancer cells by shape morphing. b The main compositions and schematic mechanism of the expansion and contraction of the pH responsive hydrogel. c 4D printing of the SMMF with designable point density in different body parts for encoding shape morphing. d SEM images and quantitative analysis of gel pores in the tail and body (inset images) of SMMF to explain the mechanism of the controllable shape morphing. e The optical images of the SMMF and SMMC opening and closing its fins and claws with the change of pH value, respectively. (Video 1). Scale bars, d 1 μm, inset images 5 μm, e 25 μm.

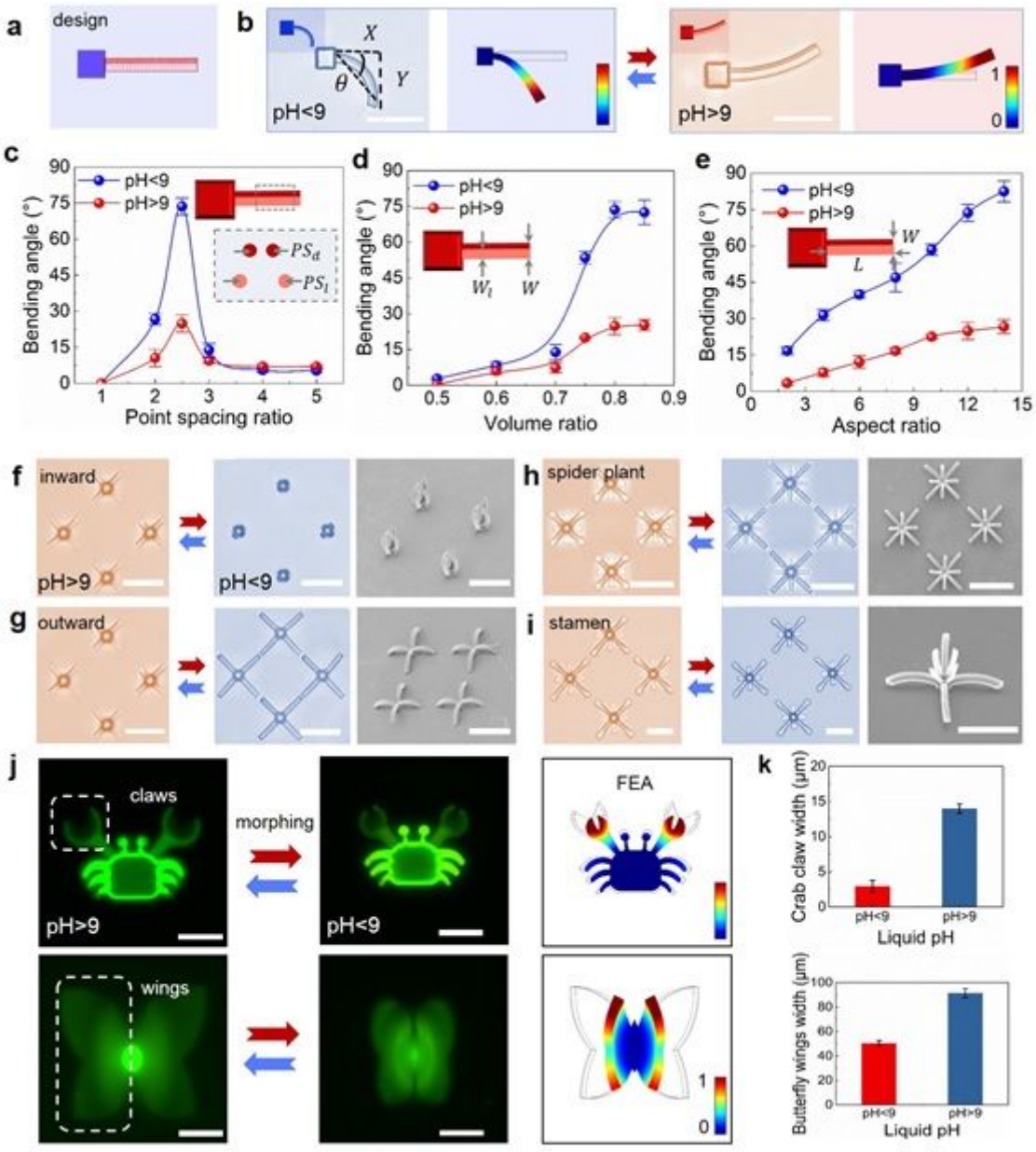

Figure 2

Programmable shape morphing of microrobots. a-b Microcantilever bending and recovering with the change of pH value, where θ is bending angle. (Video 2). c-e The quantitative relationship between bending angle and main processing parameters (VR, AR, and SPSR). f-h The optical and SEM images of microstructures bending fully inward or outward. i The optical and SEM images of microstructures bending both inward and outward together. (Video 3). j Fluorescence images of SMMC and SMMB opening and closing its claws, and wings with the change of pH value, respectively. Simulation analysis of two SMMRs are achieved for deformation predicting. k The quantitative relationship between crab claw, butterfly wings widths and pH values, respectively. All standard deviations are obtained from three parallel tests. Scale bars, a-b, 25 μm, f-i 50 μm.

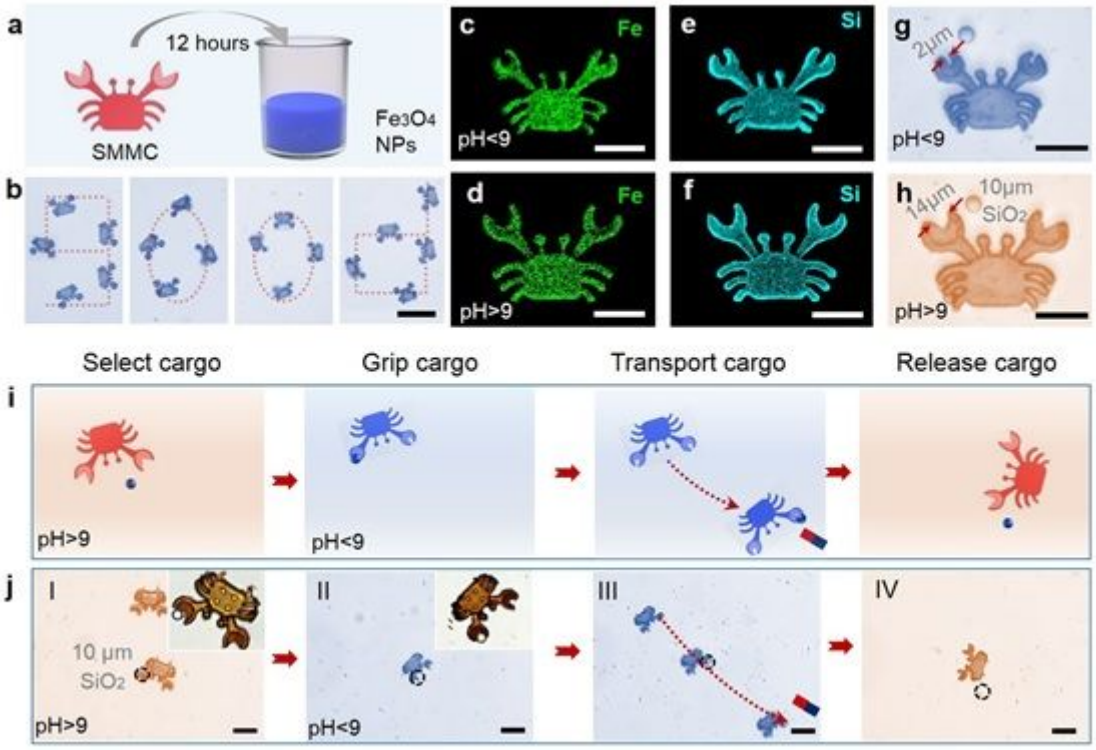

Figure 3

Magnetic SMMC for gripping, transporting and releasing microparticle by claws morphing. a Schematic illustration of the SMMC for absorbing magnetic nanoparticles in suspension. b The accurate motion control of the SMMC to form a “good” pattern by magnetic field. c-f The EDS images of the SMMC with the iron (Fe) and silicon (Si) in its body, respectively. g-h The optical images of opening and closing the SMMC claws near a microcargo, respectively. i-j The Schematic procedures and time-lapse images of selecting, tightly gripping, transporting, and releasing targeted cargo by the SMMC, respectively (Video 5). Scale bars, c-h 25 μm, j 50 μm.

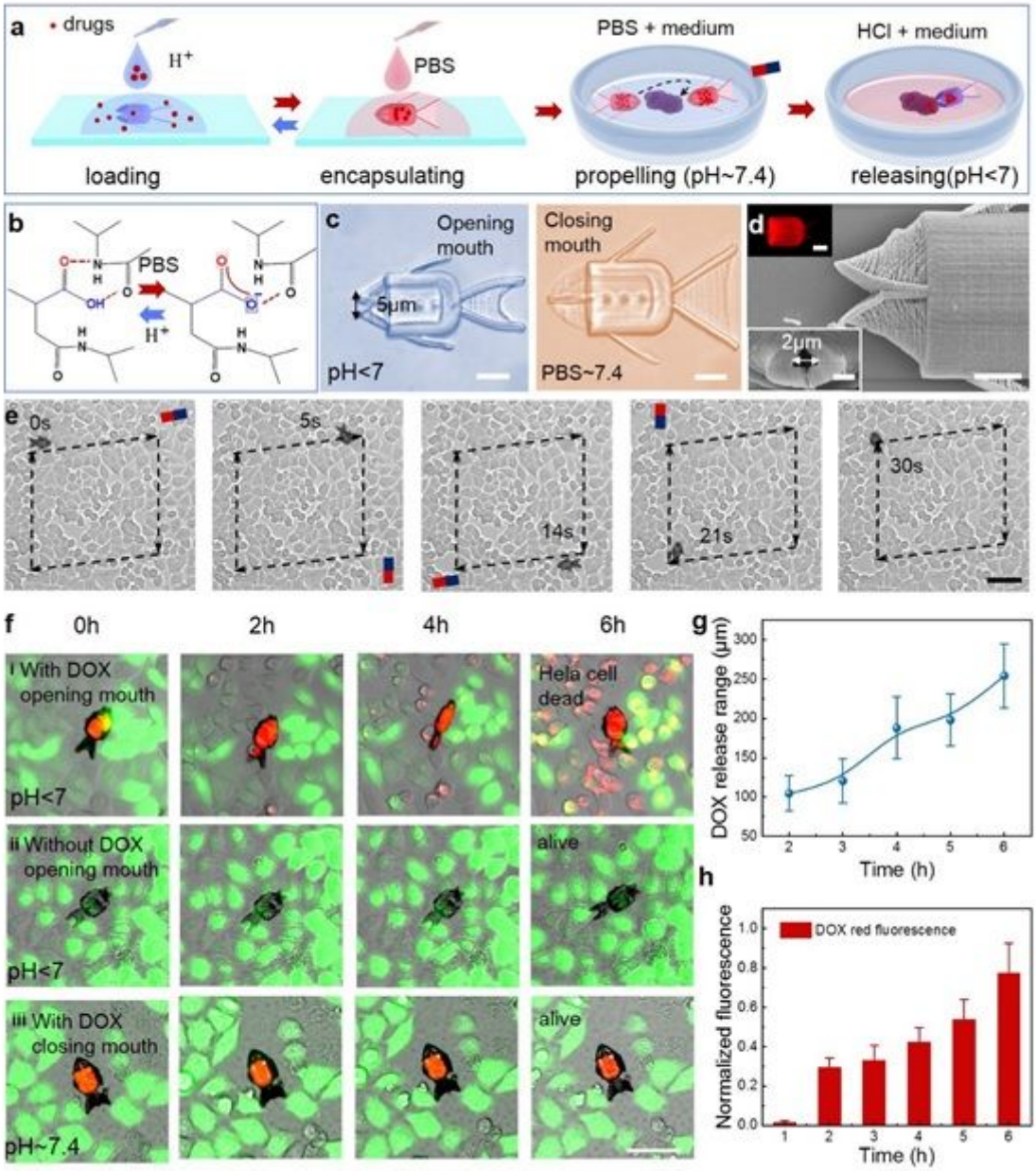

Figure 4

Magnetic SMMF encapsulating and controllable releasing drug (DOX) by mouth morphing on a cell culture plate. a Schematic of the SMMF for drugs loading, encapsulating, and delivery in vitro. b The mechanism of SMMRs swelling in PBS (pH~7.4). c-d The SMMF loading DOX by mouth morphing. The mouth of the SMMF is opened and closed in pH<7 and PBS respectively, where the red fluorescence shows the DOX encapsulated in the fish body. e Swimming of the SMMF along a designable route in a cluster of Hela cells (Video 6). f The survival status of Hela cells around SMMFs (with DOX and opening mouth, without DOX and opening mouth, with DOX and closing mouth) (Video 7). Quantitative statistics of fluorescence range (g) and intensity (h) of DOX in Hela cells, which demonstrate that the SMMF can effectively control the DOX release by opening or closing the mouth. The error bars represent the standard error of the three measurements. Scale bars, c-d 10 μm, e-f 50 μm.

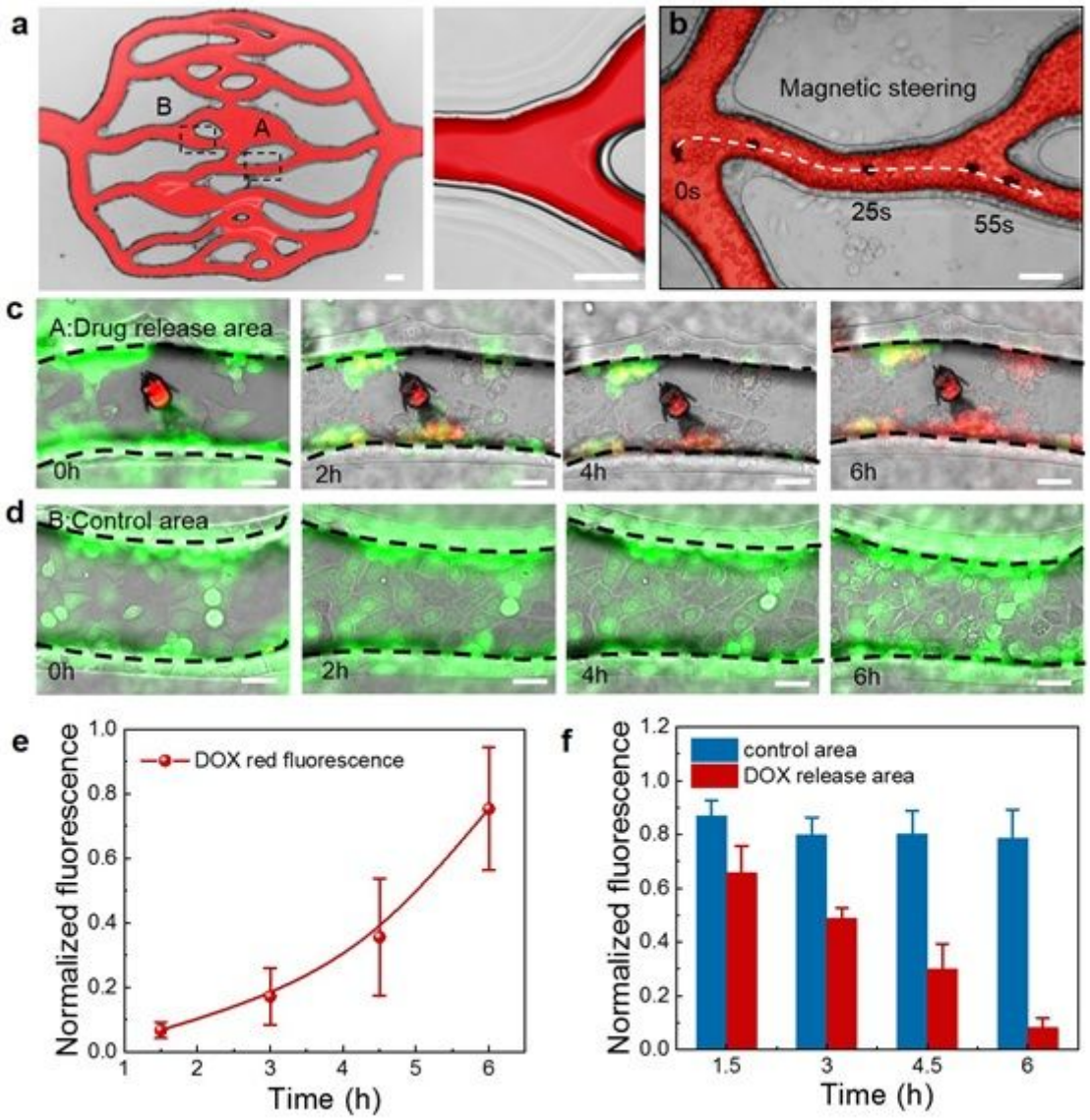

Figure 5

Localized Hela cells treatment in a complex network using magnetic SMMF. a Artificial networks by photolithography and PDMS molding. b Magnetic SMMF swimming in networks. c The snapshots of the viability of Hela cells in DOX releasing area (A in b). d the snapshots of the viability of Hela cells in control area (B in b). Quantitative statistics of releasing DOX (e) and Hela cells (f) fluorescence intensity, which demonstrate that the SMMF can kill the cancer cell by controlling the DOX release in the targeted position. The error bars represent the standard error of the three measurements. Scale bars, a-b 100 μm, c-d 25 μm.

Supplementary Files

This is a list of supplementary files associated with this preprint. Click to download.

- Video1.mp4
- Video2.mp4
- Video3.mp4
- Video6.mp4
- Video8.mp4
- Video7.mp4
- Supportinginformation.docx
- Video5.mp4
- Video4.mp4